Time Reversal Symmetry and Topology in Electromagnetics

Mário G. Silveirinha[1]

[1] University of Lisbon, Instituto Superior Técnico and Instituto de Telecomunicações, Avenida Rovisco Pais, 1, 1049-001 Lisboa, Portugal

mario.silveirinha@co.it.pt

Abstract. We present an overview of the role of time-reversal symmetry in electromagnetism and highlight how it affects the wave propagation and wave phenomena. It is shown that by combining the time-reversal symmetry with additional symmetries related to parity and duality it is possible to suppress the back-scattering in a generic bi-directional photonic platform. Furthermore, we discuss how by biasing a system with either a linear or an angular momentum one can break the time-reversal symmetry and achieve unidirectional propagation. It is discussed that the time reversal symmetry breaking is often associated with phase transitions characterized by topological invariants that determine a bulk-edge correspondence. Finally, it is highlighted that systems with continuous translation symmetry have an ill-defined topology, and that this property can be exploited to stop a wave and create energy sinks wherein the electromagnetic field is massively enhanced.

Keywords: Symmetry, Electromagnetic reciprocity, Spin Hall effect, Topological Photonics, Ill-defined topology.

1 Introduction

Time-reversal is the transformation that flips the arrow of time $t \to -t$. Notably, the laws that rule the microscopic dynamics of most physical systems are unchanged under a time-reversal. In other words, the time-reversed system state satisfies the same dynamical laws as the original state. This means that under suitable initial conditions, the time reversed dynamics may be generated and observed in a real physical scenario, analogous to a movie played backwards. In last instance, the time-reversal invariance implies that at a microscopic level the physical phenomena are reversible [1-3].

An important consequence of time-reversal invariance is that the propagation of light in typical guides is inherently bi-directional, even if the system does not have any particular spatial symmetry. For example, if some electromagnetic wave can go through a metallic pipe with no back-reflections, then the time-reversed wave also can, but propagating in the opposite direction independent of the geometry of the guide [1-3].

In this article, we present an overview of the role of time-reversal symmetry in electromagnetism and explain how it affects wave phenomena and the scattering matrix. We give a few modern examples of systems with of a broken time-reversal symmetry. Finally, we highlight the topological nature of some systems with a broken time reversal symmetry.

2 Time reversal

Consider the propagation of an electromagnetic wave in some lossless, dispersion-free, dielectric system described by the Maxwell equations:

$$\nabla \times \mathbf{E} = -\mu_0 \frac{\partial \mathbf{H}}{\partial t}, \qquad \nabla \times \mathbf{H} = \mathbf{j} + \varepsilon \frac{\partial \mathbf{E}}{\partial t}, \tag{1}$$

with $\varepsilon = \varepsilon(\mathbf{r})$. The time-reversal operation $\mathcal{T}$ transforms the electromagnetic fields $\mathbf{E}, \mathbf{H}$ and the current density $\mathbf{j}$ as $\mathbf{E} \xrightarrow{\mathcal{T}} \mathbf{E}^{\mathrm{TR}}$, $\mathbf{H} \xrightarrow{\mathcal{T}} \mathbf{H}^{\mathrm{TR}}$, and $\mathbf{j} \xrightarrow{\mathcal{T}} \mathbf{j}^{\mathrm{TR}}$ with:

$$\mathbf{E}^{\mathrm{TR}}(\mathbf{r},t) = \mathbf{E}(\mathbf{r},-t), \qquad \mathbf{H}^{\mathrm{TR}}(\mathbf{r},t) = -\mathbf{H}(\mathbf{r},-t), \qquad \mathbf{j}^{\mathrm{TR}}(\mathbf{r},t) = -\mathbf{j}(\mathbf{r},-t). \tag{2}$$

The transformed fields satisfy the same equations as the original fields. The sign of the magnetic field and of the current density is flipped under a time-reversal, and thus they are said to be odd under a time-reversal. In contrast, the electric field is unchanged and hence is even under the action of $\mathcal{T}$. Consequently, the Poynting vector $\mathbf{S} = \mathbf{E} \times \mathbf{H}$ also flips sign under a time-reversal, so that the wave dynamics and the direction of propagation are effectively reversed. The time reversal concept is rather general and applies to fields with arbitrary time dynamics.

Consider now time-harmonic solutions of the Maxwell equations, with the electromagnetic fields and the current density given by: $\mathbf{E}(\mathbf{r},t) = \mathrm{Re}\{\mathbf{E}_\omega(\mathbf{r}) e^{-i\omega t}\}$, $\mathbf{H}(\mathbf{r},t) = \mathrm{Re}\{\mathbf{H}_\omega(\mathbf{r}) e^{-i\omega t}\}$, $\mathbf{j}(\mathbf{r},t) = \mathrm{Re}\{\mathbf{j}_\omega(\mathbf{r}) e^{-i\omega t}\}$, with ω the real-valued oscillation frequency. Under a time-reversal the electric field is transformed as $\mathbf{E}(\mathbf{r},t) \to \mathrm{Re}\{\mathbf{E}_\omega(\mathbf{r}) e^{+i\omega t}\} = \mathrm{Re}\{\mathbf{E}^*_\omega(\mathbf{r}) e^{-i\omega t}\}$, where the symbol "*" stands for complex conjugation. Hence, the complex amplitudes of the fields are transformed as:

$$\mathbf{E}_\omega(\mathbf{r}) \xrightarrow{\mathcal{T}} \mathbf{E}^*_\omega(\mathbf{r}), \quad \mathbf{H}_\omega(\mathbf{r}) \xrightarrow{\mathcal{T}} -\mathbf{H}^*_\omega(\mathbf{r}), \quad \mathbf{j}_\omega(\mathbf{r}) \xrightarrow{\mathcal{T}} -\mathbf{j}^*_\omega(\mathbf{r}). \tag{3}$$

Thus, in the frequency-domain the time-reversal operation implies a phase conjugation. Similarly, voltages and currents are transformed as:

$$V_\omega \xrightarrow{\mathcal{T}} V^*_\omega, \qquad I_\omega \xrightarrow{\mathcal{T}} -I^*_\omega. \tag{4}$$

3 Scattering matrix symmetry

The time-reversal symmetry imposes several restrictions on the wave propagation and wave scattering. In what follows, it is shown that the time-reversal invariance is strictly linked to the concept of electromagnetic reciprocity. Furthermore, it is highlighted that the constraints on the scattering matrix are different for electromagnetic and condensed-matter systems.

3.1 Electromagnetic reciprocity

Consider a N-port microwave network such that the complex-amplitudes of the voltages and currents at a generic port i are of the form: $V_{\omega,i} = V_{\omega,i}^{+} + V_{\omega,i}^{-}$ and $I_{\omega,i} = \left(V_{\omega,i}^{+} - V_{\omega,i}^{-}\right)/Z_0$, i=1,…,N. Here, $V_{\omega,i}^{+}$ represents an incoming (incident) wave and $V_{\omega,i}^{-}$ an outgoing (scattered) wave. The characteristic impedance of the ports is Z_0. The incident and scattered waves are related as $\mathbf{V}^{-} = \mathbf{S}\cdot\mathbf{V}^{+}$, where $\mathbf{V}^{\pm} = \left[V_{\omega,i}^{\pm}\right]$ are column vectors and $\mathbf{S} = \left[S_{ij}\right]$ is the scattering matrix.

The time reversal operation exchanges the roles of the incident and scattered waves, such that $\mathbf{V}^{\mathrm{TR},\pm} = \mathbf{V}^{\mp,*}$. Therefore, if the system is time-reversal invariant $\mathbf{V}^{+,*} = \mathbf{S}\cdot\mathbf{V}^{-,*}$. Thus, the scattering matrix must satisfy $\mathbf{S} = \mathbf{S}^{-1,*}$. On the other hand, for a lossless system the incident power must be identical to the scattered power: $\mathbf{V}^{-}\cdot\mathbf{V}^{-,*} = \mathbf{V}^{+}\cdot\mathbf{V}^{+,*}$. In order to satisfy this additional constraint the scattering matrix must be unitary $\mathbf{S}\cdot\mathbf{S}^{\dagger} = \mathbf{1}$. Combining $\mathbf{S} = \mathbf{S}^{-1,*}$ with the unitary property, one finds that the scattering matrix must be symmetric:

$$\mathbf{S} = \mathbf{S}^{T}. \tag{5}$$

Thus, any time-reversal invariant linear lossless system is necessarily reciprocal ($S_{ij} = S_{ji}$). Electromagnetic reciprocity implies that the transmission strength from port i to port j is identical to the transmission strength from port j to port i. Thus, time-reversal invariant platforms are forcibly bi-directional.

In the previous derivation it was assumed that the system under study is lossless. This is not a limitation of the derivation, as lossy reciprocal systems have a hidden time-reversal symmetry and can be regarded as projections in real-space of a fictitious lossless system with synthetic dimensions [3]. Thus, the constraint $\mathbf{S} = \mathbf{S}^{T}$ also applies to lossy systems.

3.2 Condensed-matter systems

In electromagnetic theory the time-reversal operator $\mathcal{T}$ is idempotent, such that $\mathcal{T}^2 = \mathbf{1}$. In other words, a “double” time-reversal leaves the system state unchanged.

In contrast, in condensed matter theory –in the context of Schrödinger equation for spin ½ particles– the time-reversal operator satisfies $\mathcal{T}^2 = -\mathbf{1}$ [4]. The extra minus sign changes the phase of the wave function. This does not have any immediate physical consequences as a change of phase does not affect the expectation of physical observables. However, a careful analysis shows that the extra minus sign implies that the scattering matrix of fermionic systems is anti-symmetric [4],

$$\mathbf{S} = -\mathbf{S}^T. \tag{6}$$

This means that a time-reversal symmetric condensed matter system is matched at all its input ports, such $S_{ii} = 0$. Thus, when the number of propagating modes per physical channel is identical to one (or more generally if it is an odd number) the time-reversal symmetry enables the bi-directional propagation of electron waves free of back-scattering. This is known as the quantum spin Hall effect [4, 5].

It is relevant to mention that the minus sign in $\mathcal{T}^2 = -\mathbf{1}$ also implies that the energy states of an electronic system are forcibly degenerate. Hence, the extra minus sign is rooted in the spin degree of freedom.

4 $\mathcal{P}\cdot\mathcal{T}\cdot\mathcal{D}$ invariant systems

As previously discussed, time-reversal invariant electromagnetic platforms are characterized by a symmetric scattering matrix $\mathbf{S} = \mathbf{S}^T$. Curiously, the time-reversal symmetry does not constraint in any form the diagonal elements of the scattering matrix, which determine the reflection-loss due to the back-scattering. Evidently, it can be highly beneficial for many applications to eliminate the reflection loss. Next, we describe a class of bi-directional electromagnetic systems which are inherently matched at all input ports ($S_{ii} = 0$), analogous to spin ½ condensed matter systems.

To begin with, we write the Maxwell's equations in the frequency domain as:

$$\hat{N}\cdot\mathbf{f} = \omega\mathbf{g}, \quad \text{with} \quad \hat{N} = \begin{pmatrix} \mathbf{0} & i\nabla\times\mathbf{1}_{3\times3} \\ -i\nabla\times\mathbf{1}_{3\times3} & \mathbf{0} \end{pmatrix}. \tag{7}$$

Here, $\mathbf{1}_{3\times3}$ is the 3×3 identity matrix, ω is the oscillation frequency, $\mathbf{f} = \begin{pmatrix}\mathbf{E} & \mathbf{H}\end{pmatrix}^T$ and $\mathbf{g} = \begin{pmatrix}\mathbf{D} & \mathbf{B}\end{pmatrix}^T$ are six-component vector fields written in terms of the standard electromagnetic field vectors, and T denotes the matrix transpose operation. It is assumed that the $\mathbf{f}$ and $\mathbf{g}$ fields are linked as $\mathbf{g} = \mathbf{M}(\mathbf{r})\cdot\mathbf{f}$ where $\mathbf{M}$ is a space-dependent material matrix of the generic bianisotropic form:

$$\mathbf{M}(\omega) = \begin{pmatrix} \varepsilon_0\bar{\varepsilon} & \frac{1}{c}\bar{\xi} \\ \frac{1}{c}\bar{\zeta} & \mu_0\bar{\mu} \end{pmatrix}. \tag{8}$$

The tensors $\bar{\varepsilon}(\omega), \bar{\mu}(\omega), \bar{\xi}(\omega), \bar{\zeta}(\omega)$ are dimensionless and determine the permittivity, permeability and the magneto-electric coupling tensors, respectively.

In this compact formalism, the time-reversal operator $\mathcal{T}$ is written as $\mathcal{T} = \mathcal{K}\boldsymbol{\sigma}_z$ where $\mathcal{K}$ denotes the complex conjugation operator and $\boldsymbol{\sigma}_z = \begin{pmatrix} \mathbf{1}_{3\times3} & 0 \\ 0 & -\mathbf{1}_{3\times3} \end{pmatrix}$. The time-reversal operation transforms the (frequency domain) electromagnetic fields as $\mathbf{f} \to \mathcal{T} \cdot \mathbf{f}$ and $\mathbf{g} \to \mathcal{T} \cdot \mathbf{g}$. The operator $\mathcal{T}$ is anti-linear, i.e., it is the composition of a linear operator and $\mathcal{K}$.

The idea to mimic the behavior of condensed matter systems is to enforce suitable symmetry constraints on the material response. Specifically, it is imposed that the photonic platform is invariant under the action of some anti-linear operator $\tilde{\mathcal{T}}$, which is supposed to imitate the time-reversal operator in condensed-matter theory so that $\tilde{\mathcal{T}}^2 = -\mathbf{1}$. The operator $\tilde{\mathcal{T}}$ is required to transform the electromagnetic fields in such a manner that its action flips the Poynting vector in the relevant propagation directions, similar to the standard time-reversal operation.

A suitable operator $\tilde{\mathcal{T}}$ with the required properties is determined by the composition of the time-reversal ($\mathcal{T}$), parity ($\mathcal{P}$) and a duality transformation ($\mathcal{D}$) [5]:

$$\tilde{\mathcal{T}} = \mathcal{P} \cdot \mathcal{T} \cdot \mathcal{D}. \tag{9}$$

The parity (inversion) operator flips the *z*-spatial coordinate $(x, y, z) \to (x, y, -z)$, i.e., the coordinate perpendicular to the propagation plane (*xoy* plane). A parity operation transforms the electromagnetic fields as $\mathbf{f} \to \mathcal{P} \cdot \mathbf{f}$ and $\mathbf{g} \to \mathcal{P} \cdot \mathbf{g}$ with $\mathcal{P} = \begin{pmatrix} -\mathbf{V} & 0 \\ 0 & \mathbf{V} \end{pmatrix}$ where $\mathbf{V}$ is a 3×3 diagonal matrix with diagonal entries $V_{11} = V_{22} = -V_{33} = 1$. On the other hand, the duality transformation simply exchanges the electric and magnetic fields as $\mathbf{f} \to \mathcal{D} \cdot \mathbf{f}$ with

$$\mathcal{D} = \begin{pmatrix} 0 & \eta_0 \mathbf{1}_{3\times3} \\ -\eta_0^{-1} \mathbf{1}_{3\times3} & 0 \end{pmatrix}, \tag{10}$$

without affecting the space and the time coordinates. The $\mathbf{g}$ fields are transformed by the duality transformation as $\mathbf{g} \to -\mathcal{D}^T \cdot \mathbf{g}$. In the above, $\eta_0 = \sqrt{\mu_0 / \varepsilon_0}$ is the free-space impedance.

It can be checked that the in-plane components of the Poynting vector are flipped by the $\mathcal{P} \cdot \mathcal{T} \cdot \mathcal{D}$ transformation and that $(\mathcal{P} \cdot \mathcal{T} \cdot \mathcal{D})^2 = -\mathbf{1}$, as it should be. Furthermore, a generic photonic platform is $\mathcal{P} \cdot \mathcal{T} \cdot \mathcal{D}$ invariant when the material matrix satisfies [5]

$$\mathbf{M}(x,y,z) = -\begin{pmatrix} 0 & -\eta_0^{-1}\mathbf{V} \\ \eta_0\mathbf{V} & 0 \end{pmatrix} \cdot \mathbf{M}^T(x,y,-z) \cdot \begin{pmatrix} 0 & -\eta_0\mathbf{V} \\ \eta_0^{-1}\mathbf{V} & 0 \end{pmatrix}. \quad (11)$$

For simplicity suppose that the system is formed by lossless isotropic dielectrics, such that $\mathbf{M} = \begin{pmatrix} \varepsilon\mathbf{1}_{3\times3} & 0 \\ 0 & \mu\mathbf{1}_{3\times3} \end{pmatrix}$. Then, the $\mathcal{P}\cdot\mathcal{T}\cdot\mathcal{D}$ invariance requires simply that the relative permittivity and permeability are linked as:

$$\varepsilon(x,y,z) = \mu(x,y,-z). \quad (12)$$

An example of a $\mathcal{P}\cdot\mathcal{T}\cdot\mathcal{D}$ invariant guide is shown in Fig. 1a. The air channel is delimited by electric walls (perfect electric conductors, PEC, with $\varepsilon = -\infty$) and magnetic walls (perfect magnetic conductions, PMC, with $\mu = -\infty$). In Fig. 1, the relevant parity transformation is $(x,y,z) \to (x,-y,z)$. The plane $y=0$ is the mid-plane equidistant from the top and bottom walls. Clearly, the material parameters of two points connected by mirror symmetry are related by a duality transformation. For low frequencies, there is a single propagating mode, which turns out to be a transverse electromagnetic (TEM) wave. Therefore, provided the $\mathcal{P}\cdot\mathcal{T}\cdot\mathcal{D}$ symmetry is preserved, the guide can be arbitrarily deformed without generating any back-reflections (Fig. 1b) [5, 6, 7].

There is an apparent paradox: the platform of Fig. 1a is evidently reciprocal and thereby its scattering matrix should be symmetric $\mathbf{S} = +\mathbf{S}^T$. On the other hand, the same platform is $\mathcal{P}\cdot\mathcal{T}\cdot\mathcal{D}$-invariant and this implies that $\mathbf{S} = -\mathbf{S}^T$. A matrix can be both symmetric and anti-symmetric only if it vanishes: $\mathbf{S} = \mathbf{0}$. However, the result $\mathbf{S} = \mathbf{0}$ is evidently inconsistent with the conservation of energy in the lossless junction.

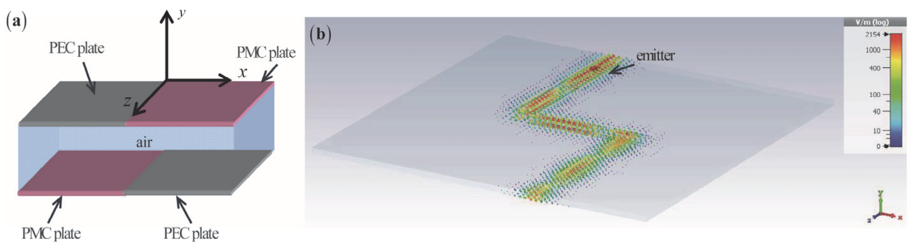

Fig. 1. (a) Sketch of a $\mathcal{P}\cdot\mathcal{T}\cdot\mathcal{D}$-invariant waveguide formed by PEC and PMC walls. The waveguide supports a mode with fields concentrated near the interface between the PEC and PMC plates. (b) Electric field profile for a zig-zag type path. If the $\mathcal{P}\cdot\mathcal{T}\cdot\mathcal{D}$ symmetry is preserved, the propagation path can be arbitrarily deformed without generating any reflections.

The solution of the paradox is that the scattering matrix is not an absolute physical object, but rather depends on the basis of modes used to expand the fields. If one chooses a basis such that $\mathbf{f}_n^- = \tilde{\mathcal{T}} \cdot \mathbf{f}_n^+$ the scattering matrix satisfies $\mathbf{S}_{\tilde{\mathcal{T}}} = -\mathbf{S}_{\tilde{\mathcal{T}}}^T$, while if one picks a basis such that $\mathbf{f}_n^- = \mathcal{T} \cdot \mathbf{f}_n^+$ the scattering matrix satisfies $\mathbf{S}_{\mathcal{T}} = +\mathbf{S}_{\mathcal{T}}^T$. Here, $\mathbf{f}_n^-, \mathbf{f}_n^+$ represent the electromagnetic fields associated with the outgoing and incoming waves on port *n*, respectively. Both scattering matrices describe equally well the relevant wave phenomena, but they are computed using two different bases of outgoing modes. Thus, electromagnetic reciprocity and the $\mathcal{P} \cdot \mathcal{T} \cdot \mathcal{D}$-symmetry are compatible, and the invariance of a system under both $\mathcal{T}$ and $\tilde{\mathcal{T}}$ does not lead to inconsistencies [5].

5 Time reversal symmetry breaking

As previously discussed, physical systems are generically time-reversal invariant at the microscopic level. Therefore, the energy-momentum dispersion has even symmetry with respect to the momentum origin: $\mathcal{E}(p) = \mathcal{E}(-p)$ (Fig. 2). This means that the energy expectation of a certain stationary state is always the same as that of the corresponding time-reversed state. Excluding the exceptional circumstance of a degenerate ground, it follows that the system "ground state" is forcibly time-reversal invariant. This property is the cornerstone of the reciprocity of standard electromagnetic platforms. Interestingly, it is possible to break the time-reversal invariance by applying a "momentum bias" that pushes the equilibrium state away from the "free-system" ground state (Fig. 2a). With an "external bias" the input-output transfer relations are not constrained by the time-reversal symmetry. The reason is that the operating point is not anymore time-reversal invariant because under a time-reversal the "momentum bias" is flipped (Fig. 2).

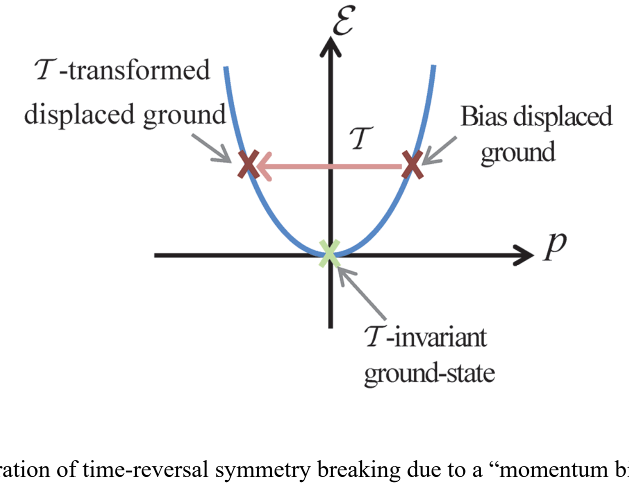

Fig. 2. Illustration of time-reversal symmetry breaking due to a "momentum bias".

There are several solutions to enforce a "momentum bias" and break the time-reversal symmetry of photonic systems [8]. The standard approach consists in biasing a material (e.g., a semiconductor or a ferrimagnetic material) with a static magnetic field. The magnetic field is transformed as $\mathbf{B} \xrightarrow{\mathcal{T}} -\mathbf{B}$ (odd quantity) under a time-reversal, i.e., similar to a "momentum". Thus, the input-output relations of a magnetically biased system are free of the time-reversal constraint. In contrast, a static electric bias does not lead directly to the time-reversal symmetry breaking because the electric field transforms as $\mathbf{E} \xrightarrow{\mathcal{T}} +\mathbf{E}$ (even quantity). However, the static electric bias can lead indirectly to a time-reversal symmetry breaking. For example, a static electric field can induce a drift-electric current in a material, which is an odd quantity under a time-reversal. Thus, systems with a drift-current bias are nonreciprocal. These ideas are developed in the following.

5.1 Static magnetic field bias

A static magnetic bias $\mathbf{B}_0$ modifies the dynamics of the electrons in a plasma through the Lorentz force. With a static magnetic bias, the motion of a generic electron with velocity $\mathbf{v}$ is determined by

$$m\frac{d\mathbf{v}}{dt} = q\left(\mathbf{E} + \mathbf{v}\times\mathbf{B}_0\right) - m\Gamma\mathbf{v}\ , \tag{13}$$

where m is the effective mass, $q = -e$ is the electron charge, Γ is the collision frequency, and $\mathbf{E}$ is the dynamical electric field. Taking $\mathbf{B}_0 = B_0\hat{\mathbf{u}}$ and assuming a time harmonic variation for $\mathbf{v}$ and $\mathbf{E}$, it follows that the averaged response of the electron gas satisfies

$$\left(\mathbf{1} + \frac{-\omega_0 i}{\omega + i\Gamma}\hat{\mathbf{u}}\times\mathbf{1}\right)\cdot\frac{\mathbf{j}}{-i\omega\varepsilon_0} = \frac{-\omega_p^2}{\omega\left(\omega+i\Gamma\right)}\mathbf{E}\ , \tag{14}$$

where $\mathbf{j} = nq\mathbf{v}$ is the electric current density, $\omega_p = \sqrt{nq^2/\varepsilon_0 m}$ is the plasma frequency and $\omega_0 = -qB_0/m = eB_0/m$ is the electron cyclotron frequency.

Solving Eq. (14) with respect to $\mathbf{j}$ and substituting the result into Faraday's equation it can be shown that the permittivity response of the biased plasma is determined by [9]:

$$\bar{\varepsilon} - \mathbf{1} = \frac{-\omega_p^2\left(\omega+i\Gamma\right)}{\omega\left(\omega+i\Gamma\right)^2 - \omega_0^2\omega}\mathbf{1}_t - \frac{i}{\omega}\frac{\omega_0\omega_p^2}{\left(\omega+i\Gamma\right)^2-\omega_0^2}\hat{\mathbf{u}}\times\mathbf{1} + \frac{-\omega_p^2}{\omega\left(\omega+i\Gamma\right)}\hat{\mathbf{u}}\otimes\hat{\mathbf{u}}\ . \tag{15}$$

This result can be written in a more compact manner as:

$$\bar{\varepsilon} = \varepsilon_t\mathbf{1}_t + \varepsilon_a\hat{\mathbf{u}}\otimes\hat{\mathbf{u}} + i\varepsilon_g\hat{\mathbf{u}}\times\mathbf{1}\ , \tag{16}$$

with

$$\varepsilon_t = 1 - \frac{\omega_p^2 \left(1 + i\Gamma / \omega\right)}{\left(\omega + i\Gamma\right)^2 - \omega_0^2}, \qquad \varepsilon_a = 1 - \frac{1}{\omega} \frac{\omega_p^2}{\left(\omega + i\Gamma\right)}, \qquad \varepsilon_g = \frac{1}{\omega} \frac{\omega_0 \omega_p^2}{\omega_0^2 - \left(\omega + i\Gamma\right)^2}. \tag{17}$$

The electromagnetic response has a broken time-reversal symmetry. In fact, flipping time requires flipping also $\mathbf{B}_0$, and thereby also the sign of ε_g. As a consequence, the electromagnetic response of a magnetized plasma is nonreciprocal ($\bar{\varepsilon} \neq \bar{\varepsilon}^T$).

The bias magnetic field bias forces the electrons to undergo circular cyclotron orbits in the bulk region with the angular frequency ω_0. The circular motion of the charged particles creates a drag-type effect when the electrons interact with a time varying field, which is at the origin of the Faraday rotation in bulk gyrotropic media. A simple way to picture the wave propagation in a magnetically biased plasma is to imagine that the wave goes through a centrifuge, e.g., rotating drum, and is dragged by the rotation of the walls. The static magnetic field effectively endows the material with an angular momentum. For example, suppose that the bias magnetic field is directed along $\hat{\mathbf{u}} = \hat{\mathbf{z}}$ with $B_0 > 0$ so that $\omega_0 > 0$. In this case, the electrons trail the cyclotron orbits in the anticlockwise direction with respect to +*z*, and thus the angular momentum of the medium is also directed along +*z*.

5.2 Unidirectional plasmons in gyrotropic media

The plasmons supported by a magnetically biased plasma can have directional properties. To illustrate this idea, consider an interface between air (in the semi-space $z > 0$) and a gyrotropic electric material (in the semi-space $z < 0$; e.g., a magnetized plasma), as depicted in Fig. 3. It is supposed that the magnetic bias is oriented along the *y*-direction ($\mathbf{B}_0 = B_0 \hat{\mathbf{u}}$ with $\hat{\mathbf{u}} = \hat{\mathbf{y}}$), i.e., it is parallel to the interface.

The short-wavelength plasmons can be found using the quasi-static approximation $\mathbf{E} \approx -\nabla \phi$, and $\mathbf{H} \approx 0$, with the electric potential satisfying $\nabla \cdot \left(\bar{\varepsilon} \cdot \nabla \phi\right) = 0$ [10]. The plane wave solutions for the electric potential (with a spatial-variation $e^{i\mathbf{k}\cdot\mathbf{r}}$) in the bulk region of the gyrotropic material must satisfy $\mathbf{k} \cdot \bar{\varepsilon} \cdot \mathbf{k} = 0$. Hence, from Eq. (16) it follows that:

$$\varepsilon_t \left(k_x^2 + k_z^2\right) + \varepsilon_a k_y^2 = 0\,. \tag{18}$$

From here, we get $ik_z = \tilde{k}_{\parallel}$ with $\tilde{k}_{\parallel} = \sqrt{k_x^2 + \frac{\varepsilon_a}{\varepsilon_t} k_y^2}$. Thus, the electric potential associated with a surface plasmon in the air-gyrotropic material interface is of the form:

$$\phi_{\mathbf{k}} = A_{\mathbf{k}_{\parallel}} e^{i\mathbf{k}_{\parallel}\cdot\mathbf{r}} \begin{cases} e^{-k_{\parallel} z}, & z > 0 \\ e^{+\tilde{k}_{\parallel} z}, & z < 0 \end{cases} \tag{19}$$

with $\mathbf{k}_{\|} = k_x \hat{\mathbf{x}} + k_y \hat{\mathbf{y}}$ the transverse wave vector, $k_{\|} = \sqrt{k_x^2 + k_y^2}$ and $A_{\mathbf{k}_{\|}}$ a normalizing factor. Imposing that the normal component of the electric displacement vector is continuous at the interface, we obtain the following dispersion equation for the natural modes:

$$-k_{\|} = k_x \varepsilon_g + \tilde{k}_{\|} \varepsilon_t \,. \tag{20}$$

When dielectric function elements depend on frequency as in Eq. (17), one gets the explicit solution [10]:

$$\omega_{\mathbf{k}} \equiv \omega_\theta = \frac{\omega_0}{2}\cos\theta + \sqrt{\frac{\omega_p^2}{2} + \frac{\omega_0^2}{4}\left(1 + \sin^2(\theta)\right)} \,. \tag{21}$$

Here, θ is the wave vector angle measured with respect to the x-axis. The function $\omega_{\mathbf{k}}$ only depends on θ, but not on the magnitude of the wave vector.
Thus, in a magnetized electron gas the resonance frequency ($\omega_{\mathbf{k}}$) of the short-wavelength plasmons is direction dependent. Furthermore, when $\omega_0 > 0$ it can be checked that $\omega_- \le \omega_{\mathbf{k}} \le \omega_+$ with

$$\omega_+ \equiv \omega_{\theta=0} = \frac{1}{2}\left(\omega_0 + \sqrt{2\omega_p^2 + \omega_0^2}\right), \tag{22a}$$

$$\omega_- \equiv \omega_{\theta=\pi} = \frac{1}{2}\left(-\omega_0 + \sqrt{2\omega_p^2 + \omega_0^2}\right). \tag{22b}$$

Note that $\omega_\pm$ determine the plasmon resonances for propagation along the x-axis, i.e., along the direction perpendicular to the magnetic bias. The asymmetry between the $+x$ and $-x$ directions is due to the magnetic field bias.

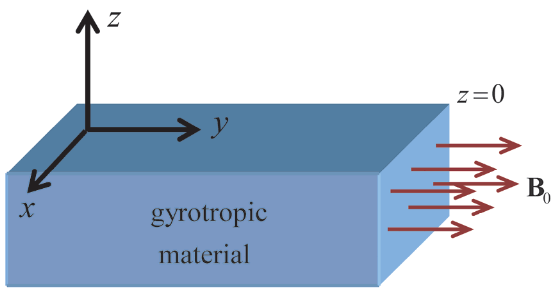

Fig. 3. Geometry of an air-gyrotropic material interface with the magnetic bias directed along the y-direction. The rotating motion of the charged particles in the bulk region drags the plasmons towards the $+x$-direction.

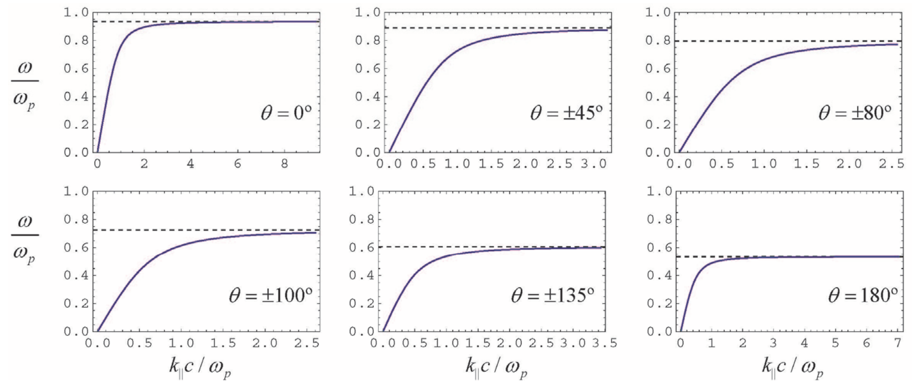

Fig. 4. Dispersion of the surface plasmons supported by an air-gyrotropic material interface for $\omega_0 = 0.4\omega_p$ along different directions of propagation θ. Solid blue lines: exact dispersion. Black dashed lines: quasi-static approximation [Eq. (21)]. Adapted from Ref. [10].

Figure 4 compares the exact plasmon dispersion with the quasi-static approximation for the case $\omega_0 = 0.4\omega_p$, showing that $\omega_\theta = \lim_{k\to\infty} \omega_{\mathbf{k}}^{\text{exact}}$. For frequencies on the order of ω_p the plasmons are effectively dragged to the semi-space $x > 0$ by the rotating motion of the electrons. This effect can lead to a regime where the surface plasmon propagation is allowed only within a sector that contains the positive *x*-axis [10, 11].

5.3 Drift-current bias

The drift-current bias is another mechanism to break the Lorentz reciprocity. However, it is usually rather impractical because significant nonreciprocal effects require large drift velocities comparable to the phase velocity of the wave. Graphene can offer a truly unique opportunity in this context: its ultra-high electron mobility may enable drift velocities on the order of $v_F = c/300$, which may be several orders of magnitude larger than the drift velocities of typical metals and several times larger than in high-mobility semiconductors [12]. A sketch of a graphene sheet biased with a drift current is shown in Fig. 5.

A drift-current endows the material with a linear momentum bias. Based on analogy with moving media, it can be shown that the effect of the drift-current bias on the graphene conductivity can be described by a Galilean-type Doppler transformation [13-15] that leads to $\sigma_{\text{g}}^{\text{drift}} = \sigma_{\text{g}}^{\text{Gal}}$ with

$$\sigma_{\text{g}}^{\text{Gal}}\left(\omega, k_x\right) = \frac{\omega}{\tilde{\omega}} \sigma_{\text{g}}\left(\tilde{\omega}, k_x\right) = i\omega\sigma_0 \frac{8}{\pi} \omega_F \frac{1}{\tilde{\omega}\sqrt{\tilde{\omega}^2 - v_F^2 k_x^2} + \tilde{\omega}^2 - v_F^2 k_x^2}. \tag{23}$$

Here, $\sigma_0 = e^2 / \left(4\hbar\right)$, $\omega_F = E_F / \hbar$ with E_F the Fermi level of graphene, $\sigma_{\text{g}}\left(\omega, k_x\right)$ is the nonlocal conductivity of graphene with no drift and $\tilde{\omega} = \omega - k_x v_0$ is the Doppler shifted frequency. We neglect interband transitions and consider the low temperature limit. Since $\sigma_{\mathrm{g}}^{\mathrm{Gal}}(\omega,k_x) \neq \sigma_{\mathrm{g}}^{\mathrm{Gal}}(\omega,-k_x)$, the drift-current biased graphene exhibits a nonreciprocal electromagnetic response.

A different model for the drift-biased conductivity is obtained by evaluating the graphene response with a skewed Fermi distribution [16, 17, 18]. The physics predicted by such a model is well captured by a relativistic-type Doppler-shift transformation [15], such that $\sigma_{\mathrm{g}}^{\mathrm{drift}} = \sigma_{\mathrm{g}}^{\mathrm{Rel}}$ with

$$\sigma_{\mathrm{g}}^{\mathrm{Rel}}(\omega,k_x) = i\omega\sigma_0 \frac{8}{\pi}\omega_F \frac{1}{\gamma(\omega - v_0 k_x)\sqrt{\omega^2 - v_F^2 k_x^2} + \omega^2 - v_F^2 k_x^2}, \tag{24}$$

where $\gamma = 1/\sqrt{1 - v_0^2 / v_F^2}$ the Lorentz factor in graphene. In our understanding, the Galilean model is more accurate than the relativistic model, as the effect of the drift-current does not change the distribution of the Bloch momentum (i.e., it does not lead to a skewed a distribution of canonical momentum), but rather changes the mean energy of the graphene electrons [15].

With a quasi-static approximation the dispersion of the graphene plasmons is determined by $q - 2\varepsilon_{\mathrm{r,s}}\kappa_{\mathrm{g}}^{\mathrm{drift}} = 0$ with $q = \sqrt{k_x^2}$ and $\kappa_{\mathrm{g}}^{\mathrm{drift}} = i\omega\varepsilon_0 / \sigma_{\mathrm{g}}^{\mathrm{drift}}$ [13]. The parameter $\kappa_{\mathrm{g}}^{\mathrm{drift}}$ can be explicitly written as

$$\kappa_{\mathrm{g}}^{\mathrm{Gal}} = \frac{1}{\alpha c 8\omega_F}\left(\tilde{\omega}\sqrt{\tilde{\omega} - v_F k_x}\sqrt{\tilde{\omega} + v_F k_x} + \tilde{\omega}^2 - v_F^2 k_x^2\right), \tag{25a}$$

$$\kappa_{\mathrm{g}}^{\mathrm{Rel}} = \frac{1}{\alpha c 8\omega_F}\left(\gamma\,\tilde{\omega}\sqrt{\omega - v_F k_x}\sqrt{\omega + v_F k_x} + \omega^2 - v_F^2 k_x^2\right), \tag{25b}$$

for the Galilean Doppler-shift and relativistic Doppler-shift models, respectively.

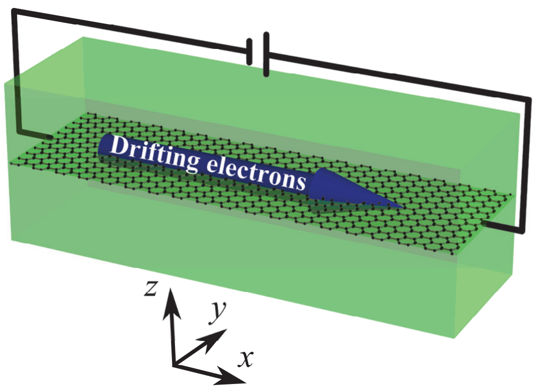

Fig. 5. Drift current biasing of graphene. A static voltage generator induces an electron drift in a graphene sheet. Adapted from Ref. [13].

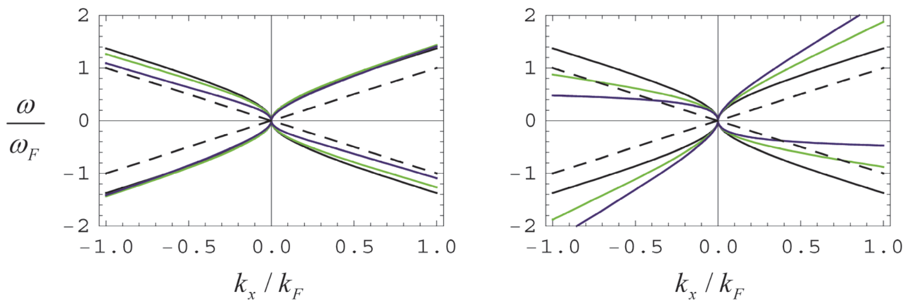

Fig. 6. Normalized dispersion of the graphene plasmons with a drift-current bias for $\varepsilon_{\mathrm{r,s}} = 4.0$ and $k_F = \omega_F / v_F$. Left: Relativistic Doppler-shift model. Right: Galilean Doppler-shift model. Black lines: $v_0 = 0$; Green lines: $v_0 = 0.5 v_F$. Blue lines: $v_0 = 0.9 v_F$. The dashed lines represent $\omega = \pm k_x v_F$.

Figure 6 shows the impact of the drift-current bias on the graphene plasmons. As seen, due to the time-reversal symmetry breaking, the dispersion suffers a blue (red) shift for plasmons co-propagating (counter-propagating) with the drifting electrons. The effect is considerably stronger in the Galilean Doppler-shift model, which predicts the emergence of unidirectional plasmon waves (see the blue lines in the right-panel of Fig. 6).

6 Topological photonics

Topology studies the properties of objects that stay invariant under a continuous transformation. When some property of a mathematical object is unaffected by a deformation it is called a topological invariant. For example, in the theory of surfaces the number of holes is a topological invariant known as the genus. Any continuous deformation of the surface must preserve the genus, which is thereby a global property fully independent of any local features of the surface.

It is possible to characterize the topology of other more abstract mathematical objects, e.g., Hermitian operators, for which the topological invariants do not have an immediate geometrical visualization [19]. Next, we focus on the characterization of the topological phases of lossless electromagnetic continua.

6.1 Topological classification of electromagnetic continua

The topological classification of physical systems is rooted in the cyclic structure of the wave vector space [19]. Indeed, to ensure that the topological invariant –the Chern number– is an integer, it is necessary that the underlying space is a closed surface with no boundary. In a periodic system the relevant space is the Brillouin zone, which is isomorphous to a torus.

It is relevant to extend topological ideas to physical systems with no intrinsic periodicity, e.g., to metamaterials modeled by some effective parameters [20]. Indeed, the electrodynamics of continuous media is much simpler than that of periodic structures, and this simplicity may give additional physical insights and a deeper understanding of topological photonics. Similar to periodic systems, due to the frequency dispersion of the material response, continuous media are also characterized by an intricate band structure. However, unlike in periodic structures, for continuous media the wave vector space is an unbounded open region (the Euclidean space). In Ref [20], it was shown that despite this unusual feature it is possible to characterize the topological phases of electromagnetic systems when a suitable regularization process is applied to the material response.

Specifically, the response of a material described by the local material matrix $\mathbf{M}(\omega)$ can be regularized as follows:

$$\mathbf{M}_{\text{reg}}(\omega,\mathbf{k}) = \mathbf{M}_\infty + \frac{1}{1+k^2/k_{\text{max}}^2}\left[\mathbf{M}(\omega)-\mathbf{M}_\infty\right], \qquad (26)$$

where $\mathbf{M}_\infty = \lim_{\omega\to\infty}\mathbf{M}(\omega)$. Here, k_{max} is a high-frequency wave vector cut-off, which can be arbitrarily large. The regularized material response is evidently spatially dispersive (nonlocal), as it depends on the wave vector $\mathbf{k}$. Clearly, for $k << k_{\text{max}}$ the transformed material matrix is nearly coincident with the original material matrix: $\mathbf{M}_{\text{reg}}(\omega,\mathbf{k}) \approx \mathbf{M}(\omega)$. The cut-off ensures that as $k\to\infty$ the material response approaches that of vacuum ($\lim_{k\to\infty}\mathbf{M}_{\text{reg}}(\omega,\mathbf{k}) = \mathbf{M}_\infty$), similar to what happens in the $\omega\to\infty$ limit.

The physical justification to introduce a cut-off is that in a realistic material a field with a very fast spatial variation cannot effectively polarize the microscopic constituents of the medium, and hence the material response is expected to vanish when $k\to\infty$.

Figure 7 depicts the band diagram of an electric gyrotropic material with $\hat{\mathbf{u}} = \hat{\mathbf{z}}$ (see Eq. (16)) and the permittivity elements:

$$\varepsilon_t = 1+\frac{\omega_0\omega_e}{\omega_0^2-\omega^2}, \qquad \varepsilon_g = \frac{\omega_e\omega}{\omega_0^2-\omega^2}, \qquad \varepsilon_a = 1. \qquad (27)$$

In the above, $|\omega_0|$ is the resonance frequency and ω_e determines the resonance strength. The parameter ω_0 may be either positive or negative and it is necessary that $\omega_0\omega_e > 0$. The dispersion of transverse magnetic (TM) waves with $E_z = 0$ and $H_z \neq 0$ is given by:

$$k_x^2 + k_y^2 = \frac{\varepsilon_t^2-\varepsilon_g^2}{\varepsilon_t}\left(\frac{\omega}{c}\right)^2. \qquad (28)$$

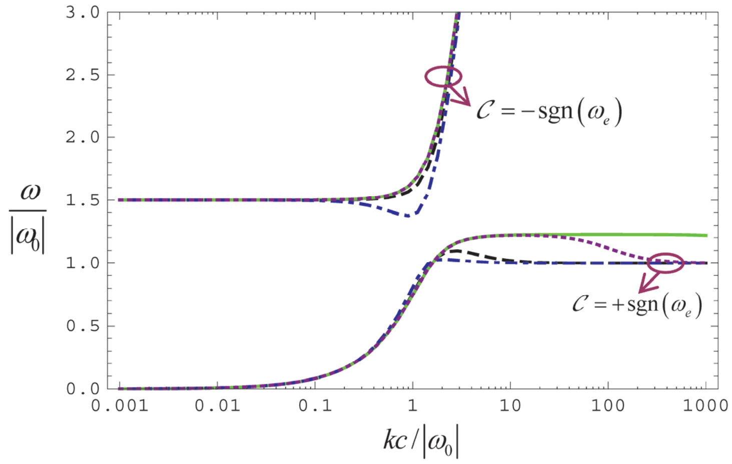

Fig. 7. Effect of the high-frequency spatial cut-off on the band structure ω vs. k of a gyrotropic material with $\omega_e = 0.5\omega_0$ and (i) (green solid lines) no spatial-cut off, (*iii*) (purple dotted lines) $k_{max} = 100|\omega_0|/c$, (*iii*) (black dashed lines) $k_{max} = 3|\omega_0|/c$, and (*iv*) (blue dot-dashed lines) $k_{max} = |\omega_0|/c$. Adapted from Ref. [20].

As seen in Fig. 7, for $k << k_{max}$ the band structure calculated with the cut-off (purple, black and blue lines) is nearly coincident with the band structure of the original gyrotropic material (green lines, for $k_{max} = \infty$). By increasing k_{max} the coincidence can be made as good as one may wish. For $k >> k_{max}$, the band structure inevitably depends on the spatial cut-off.

Notably, when the spatial cut-off is enforced the Chern numbers are always integer numbers. The Chern invariants are calculated as explained in Ref. [20], including the wave vector cut-off in the permittivity response of the material. It turns out that independent of the value k_{max} (at least for a sufficiently large k_{max}) the Chern invariant of the high-frequency band is $\mathcal{C}_n = -\mathrm{sgn}(\omega_e)$, and the Chern invariant of the low-frequency band is $\mathcal{C}_n = +\mathrm{sgn}(\omega_e)$. In practice, the sign of ω_e depends on the direction of a bias magnetic field.

6.2 Bulk-edge correspondence

The most celebrated property of topological systems is the bulk-edge correspondence [21-23]. It establishes that when two inequivalent topological materials are paired the corresponding material interface must forcibly support a net number of *unidirectional* edge states determined by the difference of the gap Chern numbers of the bulk materials. Furthermore, the edge states are gapless and hence their dispersion must cross the common band-gap.

6.3 Ill-defined topologies and energy sinks

From the previous subsections, it is clear that some physical systems cannot be topologically classified even though their spectrum has a full band-gap. This property can be explained in a geometrical way. Specifically, consider the mathematical objects represented in Fig. 8a. The objects on the left and right panels have a well defined topology determined by the genus of the corresponding surface. In contrast, the object in the middle panel has an ill-defined topology. Indeed, the cross-sectional cut of a torus with vanishing inner radius consists of two-kissing circles, and, thereby the number of holes of the surface is indefinite.

Ill-defined topologies arise naturally in the study of the wave propagation in physical systems with a continuous translational symmetry. Indeed, consistent with Sect. 6.1 the topological classification of continuum models requires the regularization of the system response with some high-spatial frequency cut-off. Without the spatial cut-off, the topology is ill-defined in the same manner as the topology of the torus with vanishing inner radius is ill-defined. A practical consequence of this is that the wave propagation in such systems is not constrained by the bulk-edge correspondence principle [22]. Mathematically the pathologic situation arises due to the continuous translational symmetry of the material.

Remarkably, an ill-defined topology creates an opportunity to stop a wave in a carefully designed electromagnetic waveguide, leading to the formation of hotspots where the electromagnetic fields are massively enhanced [24]. This idea is illustrated in Fig 8b which represents an edge-type unidirectional (horizontal) waveguide formed by a PEC wall and a gyrotropic material with an ill-defined topology. Interestingly, an interface of the same gyrotropic material and a PMC wall does not support propagating states. This is only possible due to the breakdown of the bulk-edge correspondence in media with an ill-defined topology [22].

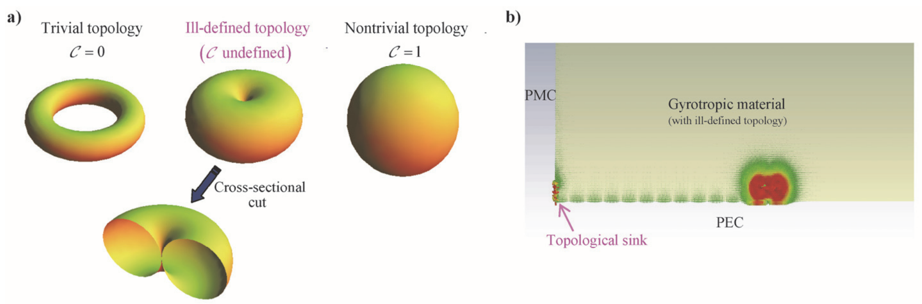

Fig. 8. a) Geometrical illustration of the concept of an ill-defined topology. The torus and the sphere on the left and right panels have well defined topologies determined the number holes of each surface. In contrast a torus with a vanishingly small inner radius (middle panel) has an ill-defined topology. b) A nonreciprocal material with a continuous translational symmetry has an ill-defined topology, and can be used to realize a topological energy sink that drags towards its interior the radiation generated in the surroundings.

The breakdown of the bulk-edge correspondence creates a deadlock for the unidirectional edge mode propagating in the horizontal guide. At the junction point, the incoming wave has no place to go: it cannot propagate to the vertical PMC wall, it cannot escape to the bulk regions and it cannot be back-reflected because the edge mode is unidirectional and immune to backscattering. Therefore, in the idealized case of lossless materials, the electromagnetic energy is forced to accumulate at the vertex point of the PEC and PMC walls. Thus, ill-defined topologies can lead to the formation of energy sinks with ultra-singular fields that absorb all the energy generated in their surroundings. Such systems can be useful, for example, for energy harvesting or to enhance nonlinearities [24].

References

1. Feynman, R., Leighton, R., Sands, M.: The Feynman lectures on physics, California Institute of Technology, (1963).
2. Silveirinha, M. G.: Time-reversal symmetry in Antenna Theory, Symmetry, 11, 486, (2019).
3. Silveirinha, M. G.: Hidden Time-Reversal Symmetry in Dissipative Reciprocal Systems, Opt. Express, 27, 14328, (2019).
4. Shen, S.-Q.: Topological insulators, Solid State Sciences Vol. 174, Springer, Berlin, 2012, p. 98.
5. Silveirinha, M. G., PTD Symmetry Protected Scattering Anomaly in Optics, Phys. Rev. B, 95, 035153, (2017).
6. Martini, E., Silveirinha, M. G., Maci, S.: Exact Solution for the Protected TEM edge mode in a PTD-Symmetric Parallel-Plate Waveguide, IEEE Trans. Antennas and Propag., 67, 1035-1044, (2019).
7. Chen, W.-J., Zhang, Z.-Q., Dong, J.-W., Chan, C.T.: Symmetry-protected transport in a pseudospin-polarized waveguide, Nat. Comm., 6, 8183, (2015).
8. Caloz, C., Alù, A., Tretyakov, S., Sounas, D., Achouri, K., Deck-Léger, Z.-L.: Electromagnetic Nonreciprocity, Phys. Rev. Applied, 10, 047001, (2018).
9. Bittencourt, J. A.: Fundamentals of Plasma Physics, 3rd edn. Springer-Verlag, New York, (2010).
10. Silveirinha, M. G., Gangaraj, S. A. H., Hanson, G. W., Antezza, M.: Fluctuation-induced forces on an atom near a photonic topological material, Phys. Rev. A, 97, 022509, (2018).
11. Gangaraj, S. A. H., Hanson, G. W., Silveirinha, M. G., Shastri, K., Antezza, M., and Monticone, F.: Truly unidirectional excitation and propagation of difractionless surface plasmon-polaritons, Phys. Rev. B., 99, 245414, (2019).
12. Gonçalves, P. A. D.; Peres, N. M. R.: An introduction to graphene plasmonics; World Scientific, Hackensack, NJ, 2016.
13. Morgado, T. A., Silveirinha, M. G.: Drift-induced Unidirectional Graphene Plasmons, ACS Photonics, 5, 4253, (2018).
14. Morgado, T. A., Silveirinha, M. G.: Negative Landau damping in bilayer graphene, Phys. Rev. Lett., 119, 133901, (2017).
15. Morgado, T. A., Silveirinha, M. G.: Reply to comment on “Negative Landau Damping in Bilayer Graphene”, Phys. Rev. Lett., 123, 219402, (2019).
16. Borgnia, D. S., Phan, T. V., Levitov, L. S.: Quasi-Relativistic Doppler Effect and Non-Reciprocal Plasmons in Graphene, arXiv: 1512.09044.

17. Van Duppen, B., Tomadin, A., Grigorenko, A. N., Polini, M.: Current-induced birefrigent absorption and non-reciprocal plasmons in graphene, 2D Mater. 3, 015011 (2016).
18. Wenger, T., Viola, G., Kinaret, J., Fogelström, M., Tassin, P.: Current-controlled light scattering and asymmetric plasmon propagation in graphene, Phys. Rev. B 97, 085419 (2018).
19. Ozawa, T., Price, H. M., Amo, A., Goldman, N., Hafezi, M., Lu, L., Rechtsman, M. C., Schuster, D., Simon, J., Zilberberg, O., Carusotto, I.: Topological photonics, Rev. Mod. Phys. 91, 015006, (2019).
20. Silveirinha, M. G.: Chern Invariants for Continuous Media, Phys. Rev. B, 92, 125153, (2015).
21. Hatsugai, Y.: Chern number and edge states in the integer quantum Hall effect, Phys. Rev. Lett. 71, 3697, (1993).
22. Silveirinha, M. G.: Bulk edge correspondence for topological photonic continua, Phys. Rev. B, 94, 205105, (2016).
23. Silveirinha, M. G.: "Proof of the bulk-edge correspondence through a link between topological photonics and fluctuation-electrodynamics", Phys. Rev. X, 9, 011037, (2019).
24. Fernandes, D. E., Silveirinha, M. G.: Topological origin of electromagnetic energy sinks, Phys. Rev. Appl., 12, 014021, (2019).